NANO LETTERS

Letter

pubs.acs.org/NanoLett

Visible Surface Plasmon Modes in Single Bi_2Te_3 Nanoplate

Meng Zhao,[†,‡] Michel Bosman,[§] Mohammad Danesh,[∥,#] Minggang Zeng,[‡,▽] Peng Song,[†,‡] Yudi Darma,[⊥,▽] Andrivo Rusydi,[⊥,▽] Hsin Lin,[‡,▽] Cheng-Wei Qiu,[∥] and Kian Ping Loh*[,†,‡]

[†]Department of Chemistry, National University of Singapore, 3 Science Drive 3, 117543, Singapore

[‡]Centre for Advanced 2D Materials and Graphene Research Centre, National University of Singapore, 6 Science Drive 2, 117546, Singapore

[§]Institute of Materials Research and Engineering, A*STAR (Agency for Science, Technology and Research), 2 Fusionopolis Way, 138634, Singapore

[∥]Department of Electrical and Computer Engineering, National University of Singapore, 4 Engineering Drive 3, 117583, Singapore

[#]Electronics and Photonics Department, Institute of High Performance Computing, 1 Fusionopolis Way, 138632, Singapore

[▽]Department of Physics, National University of Singapore, 2 Science Drive 3, 117542, Singapore

[⊥]Singapore Synchrotron Light Source, National University of Singapore, 5 Research Link, 117603, Singapore

Supporting Information

ABSTRACT: Searching for new plasmonic building blocks which offer tunability and design flexibility beyond noble metals is crucial for advancing the field of plasmonics. Herein, we report that solution-synthesized hexagonal Bi_2Te_3 nanoplates, in the absence of grating configurations, can exhibit multiple plasmon modes covering the entire visible range, as observed by transmission electron microscopy (TEM)-based electron energy-loss spectroscopy (EELS) and cathodoluminescence (CL) spectroscopy. Moreover, different plasmon modes are observed in the center and edge of the single Bi_2Te_3 nanoplate and a breathing mode is discovered for the first time in a non-noble metal. Theoretical calculations show that the plasmons observed in the visible range are mainly due to strong spin−orbit coupling induced metallic surface states of Bi_2Te_3. The versatility of shape- and size-engineered Bi_2Te_3 nanocrystals suggests exciting possibilities in plasmonics-enabled technology.

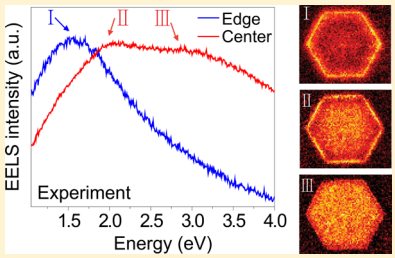

KEYWORDS: *Bi_2Te_3, surface plasmon, visible, electron energy-loss spectroscopy, cathodoluminescence, spin−orbit coupling*

Surface plasmons are electromagnetic waves arising from collective oscillations of electrons at the interface of a metal and a dielectric. They can confine light into subwavelength volumes and propagate along the surface.[1] Surface plasmons in the visible range have been the topic of numerous studies due to their appealing applications in various fields, such as photovoltaics,[2] sensing,[3−5] and waveguides.[6,7] However, the choice of materials that can support surface plasmons in the visible range is largely limited to noble metals; thus, there are strong motivations to search for novel plasmonic materials beyond gold and silver.

Bi_2Te_3 and its alloys are well-known for their outstanding thermoelectric properties.[8,9] In the past decade, this traditional semiconductor material has attracted intense interests since it was discovered to be a three-dimensional (3D) topological insulators (TIs).[10,11] TIs are materials which behave as insulators in the bulk but have metallic surfaces with a single Dirac cone. 3D TIs have also drawn interest as emerging novel plasmonic materials recently. Lupi et al. discovered plasmonic resonances on Bi_2Se_3 gratings in the far-infrared range,[12] while Nikolay et al. reported ultraviolet (UV) to visible plasmons in periodic nanostructures fabricated on $Bi_{1.5}Sb_{0.5}Te_{1.8}Se_{1.2}$.[13] It should be noted that the reported plasmon resonances were excited by fabricating periodic gratings on TI thin films, and detected by optical spectroscopy. Real space imaging of plasmon in these materials is not achieved yet.

Understanding the physics embodied in optical phenomena at the nanoscale helps to drive the development of photonic and plasmonic devices. Optical dark-field microscopy (DFM) and near-field scanning optical microscopy (NSOM) are commonly used to characterize the electromagnetic field distribution of surface plasmons in nanostructures.[14−17] Complementary to DFM and NSOM, TEM-EELS and TEM-CL are powerful tools for studying plasmons in nanostructures with high spatial (<1 nm) and energy resolution (<0.1 eV), with the ability to map the plasmon field distributions.[18−21] Moreover, optically forbidden excitations such as dark plasmon modes can be accessed by TEM-EELS, where insights about near field coupling can be obtained.[22−24]

In this study, we synthesized Bi_2Te_3 nanoplates using the solvothermal method and characterized the intrinsic surface plasmon resonances on individual Bi_2Te_3 nanoplates, excluding grating effects due to the periodic structure. Taking advantage of the high spatial precision and energy resolution of TEM-

Received: September 29, 2015
Revised: November 11, 2015
Published: November 16, 2015

DOI: 10.1021/acs.nanolett.5b03966
Nano Lett. 2015, 15, 8331−8335

EELS and TEM-CL, the spatial distribution of plasmon modes supported on a single nanoplate was fully characterized. Our studies revealed that a hexagonal Bi_2Te_3 nanoplate can support surface plasmons in the entire visible range from 1.6 to 3.1 eV (400−800 nm) and we obtained real space imaging of the plasmon modes in TI for the first time. Different modes were observed in the center and edge of the nanoplate, and a dark breathing plasmon mode excited in the center was first discovered in non-noble metal plasmonic materials. Density functional theory calculations show that all the observed plasmon modes are related to the strong spin−orbit coupling induced surface states of Bi_2Te_3.

The Bi_2Te_3 nanoplates were synthesized by the solvothermal method, in which Bi_2O_3 and TeO_2 were used as the precursors, ethylene glycol as the major solvent and reducing agent, and polyvinylpyrrolidone (PVP) as the surfactants.[25] As shown in the scanning electron microscopy (SEM) image (Figure 1a), a high yield of hexagonal Bi_2Te_3 nanoplates with lateral widths of 550−700 nm was obtained. The crystal size can be tuned between 50 and 1000 nm by adding another reducing solvent, such as isopropyl alcohol or glycerol (see Figure S1). The crystal structure of the Bi_2Te_3 nanoplates was analyzed using X-ray diffraction (XRD), the results of which are shown in Figure 1b. All diffraction peaks in the Bi_2Te_3 XRD pattern can be indexed to a single rhombohedral phase with lattice constants a = 4.395 Å and c = 30.44 Å (JCPDS Card Number 82−0358). The topographical images obtained by atomic force microscopy (AFM) reveal that the nanoplates have very flat surfaces (Figure 1c and Figure S2). The thickness distribution was determined by measuring 75 randomly chosen nanoplates. As seen in Figure 1d, most of the nanoplates have thicknesses of 15 ± 5 nm. UV−Vis absorption spectrum of Bi_2Te_3 nanoplates (Figure S3) dispersed in isopropyl alcohol shows broad and strong absorption in the visible range, which motivates us to further investigate plasmonic properties of individual Bi_2Te_3 nanoplates in detail.

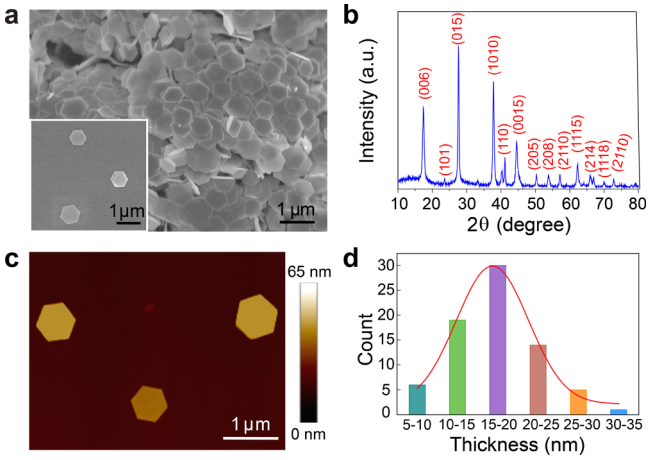

Figure 1. Characterizations of the as-synthesized Bi_2Te_3 nanoplates. (a) SEM image showing clusters of and individual (insert) Bi_2Te_3 nanoplates. (b) XRD spectrum with peak assignment. (c) Topographical AFM image of three uniform nanoplates. (d) Thickness distribution from a random sample of 75 nanoplates.

Individual nanoplates were characterized using a scanning transmission electron microscope (STEM) equipped with a monochromator and an electron energy-loss (EEL) spectrometer. Bi_2Te_3 nanoplates were drop-cast onto a 30 nm thick silicon nitride membrane and then annealed under Ar/H_2 atmosphere to remove impurities and the oxidized layer. The EELS measurements were carried out using an FEI Titan TEM equipped with a Schottky electron source in STEM mode, operated at 80 kV for all measurements (see Supporting Information for more details). Figure 2a shows a TEM micrograph of a hexagonal Bi_2Te_3 nanoplate with a lateral dimension of ∼700 nm. Strain-induced ripple-like patterns can be seen. The sharp diffraction spots in the selected area electron diffraction (SAED) pattern and the hexagonal lattice arrangements in the high resolution TEM (HRTEM) image (Figure 2, parts b and c) indicate that the nanoplate is single-crystalline. Experimental EEL spectra of the Bi_2Te_3 nanoplate are shown in Figure 2d. When the electron beam was positioned near the edge of the nanoplate (about 2 nm away from the edge in practice), an energy-loss peak at 1.6 eV was observed (mode I). Moving the electron beam from the edge to the center of the nanoplate resulted in a broad EEL spectrum with energy-loss peaks at 2.1 eV (mode II) and at 3.1 eV (mode III). The losses observed in EEL spectra can be associated with various forms of loss mechanisms occurring between the impinging electron beam and the Bi_2Te_3 crystal, including

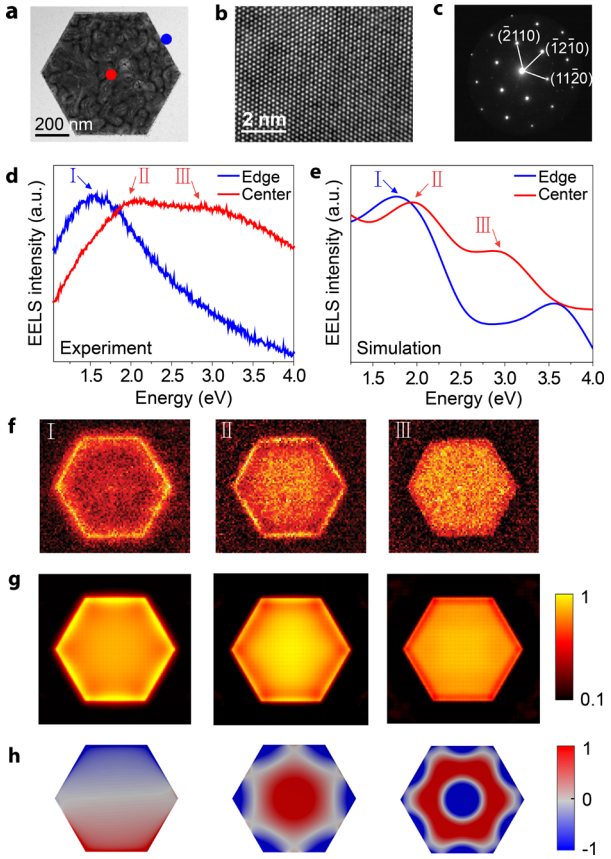

Figure 2. Surface plasmon modes of a hexagonal Bi_2Te_3 nanoplate. (a) TEM image of the hexagonal Bi_2Te_3 nanoplate. (b) High resolution TEM (HRTEM) image of the nanoplate and the corresponding SAED pattern (c). (d) EELS of the nanoplate when the electron beam is positioned at the middle of the edge (blue line) and center (red line) of the nanoplate, corresponding to the blue and red dots in part a. (e) Corresponding simulation results using COMSOL. (f) Experimental EELS maps, (g) calculated field intensity, and (h) charge distribution of the nanoplate at different energies corresponding to the three peaks in part d.

DOI: 10.1021/acs.nanolett.5b03966
Nano Lett. 2015, 15, 8331−8335

surface and bulk plasmon modes.[18] We assign these to surface plasmon resonance modes, instead of bulk plasmons that are expected to appear at higher energies and exhibit spatially homogeneous EELS intensity with no size dependence (see later sections).[26,27]

EELS mapping was performed to gain insight into the spatial distribution of the plasmon modes.[28,29] Figure 2f shows the EELS intensity maps at 1.6, 2.1, and 3.1 eV, corresponding to the three peaks shown in Figure 2d. As shown in Figure 2f, the 1.6 eV mode occurs only at the edges of the nanoplate, with an obvious evanescent wave field decaying into the vacuum, a phenomenon which is characteristic of localized surface plasmons.[30] The map of the center mode II shows enhanced EELS intensity not only in the center, but also at the edges of the nanoplate. The center mode III at 3.1 eV is delocalized over the entire nanoplate except the edges.

The EEL spectra and maps were simulated by performing full wave calculations of the scattered fields using the finite element method with the commercial software COMSOL and the boundary element method incorporated in the MNPBEM toolbox.[31] The dielectric function of Bi_2Te_3 was extracted from ellipsometry data. The simulation model used a 10 nm-thick hexagonal Bi_2Te_3 crystal on top of a 30 nm-thick Si_3N_4 substrate. Parts e and g of Figure 2 show the simulated EEL spectra and maps of a Bi_2Te_3 hexagonal nanoplate with lateral dimension of 700 nm, respectively. Generally, both the spectral and spatial features are well matched between the simulation and experiments. The slight deviation may be attributed to the thickness variation and surface residues.[28] To understand the origin of these modes, charge distributions of each plasmon mode were simulated (Figure 2h). The edge mode I exhibits a strong charge localization at the edges of the crystal, creating a dipolar electric polarizability along the nanoplate. On the other hand, the center mode II shows very different resonance behavior, which is induced by charge oscillations between the nanoplate center and the edges. The hexagonal shape provides a broad length range in which the charge can oscillate to/from the center, varying from the short-distance center-to-edge to the long-distance center-to-corner radius of the hexagon, creating a broadened center mode.

A plasmon mode of particular interest is the center mode at 3.1 eV. The simulated charge distribution of this mode shows that the charge density radially oscillates toward the edges, which is characteristic of the so-called "breathing mode" surface plasmon.[23,32] A breathing mode is a two-dimensional standing wave with an antinode at the center of the nanoplate.[23] It is classified as a dark surface plasmon mode, as it cannot be excited by unpolarised and normal incident light due to its zero net dipole moment.[32] For plasmon-enabled applications, identification of dark plasmon modes is important because of their capability to store electromagnetic energy more efficiently than bright modes, as a result of the suppression of the radiative decay channel.[33] The hexagonal shape and large size of Bi_2Te_3 nanostructures allow radially oscillating charges on the surface, giving rise to plasmonic breathing modes.[32]

Cathodoluminescence spectroscopy (CL), which collects the photon-emissions in the far field resulting from the radiative decay of plasmon modes,[18] was also applied to characterize the plasmon modes in Bi_2Te_3 nanoplates (Figure 3a). When the electron beam was positioned at the center of the 700 nm nanoplate (No. 6 in Figure 3a), a broad peak centered at 2.1 eV was observed, which is consistent with mode II recorded with EELS. However, the 3.1 eV peak observed in the EELS is

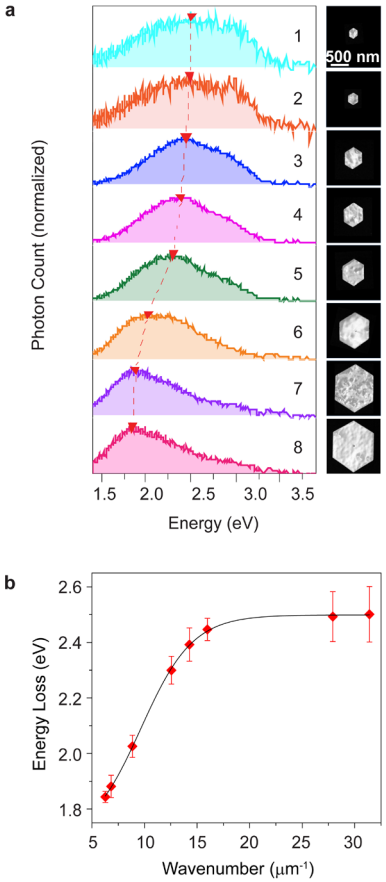

Figure 3. CL spectra of Bi_2Te_3 nanoplates. (a) CL spectra at the center and the corresponding high-angle annular dark field (HAADF) image of Bi_2Te_3 nanoplates with different size. (b) Dispersion relation of the center mode surface plasmons (error bars represent uncertainty in determining CL peak energy).

absent in the CL spectrum. As the mode of 3.1 eV is a breathing mode surface plasmon, of which the main decay channel is the absorption by the particle,[18] it cannot be detected in far field by CL spectroscopy. The mode assignment is consistent with the observed broad spectral features, due to strong radiative damping of the mode.[34,35]

We also studied how the center mode changes with nanoplates of different sizes. Figure 3a shows that the plasmon energy exhibits a monotonous red-shift when the nanoplate size increases from 200 to 1000 nm. The plasmon wavenumber (k_{SP}) of this mode can be described using the equation

$$k_{SP} = 2\pi/\lambda_{SP} = 2\pi/d$$

where d corresponds to the effective diameter of the nanoplate.[36] Accordingly, we derive the dispersion relation by plotting the plasmon frequency (extracted from the peak positions in Figure 3a) as a function of the wavenumber k_{SP} in Figure 3b. The curve asymptotically approaches an energy value of about 2.5 eV, displaying the characteristic dispersion relation of surface plasmons. Further measurements of size dependence (see Figure S4) reveal that both the edge and center modes red-shift with increasing nanoplate size, similar to the plasmonic behavior of noble metal nanostructures.[37,38]

The origin of visible surface plasmons in Bi_2Te_3 was examined by measuring the dielectric function of a thin layer of the Bi_2Te_3 nanoplates using ellipsometry (Figure 4a). To support surface plasmons at the interface between a medium

DOI: 10.1021/acs.nanolett.5b03966
Nano Lett. 2015, 15, 8331−8335

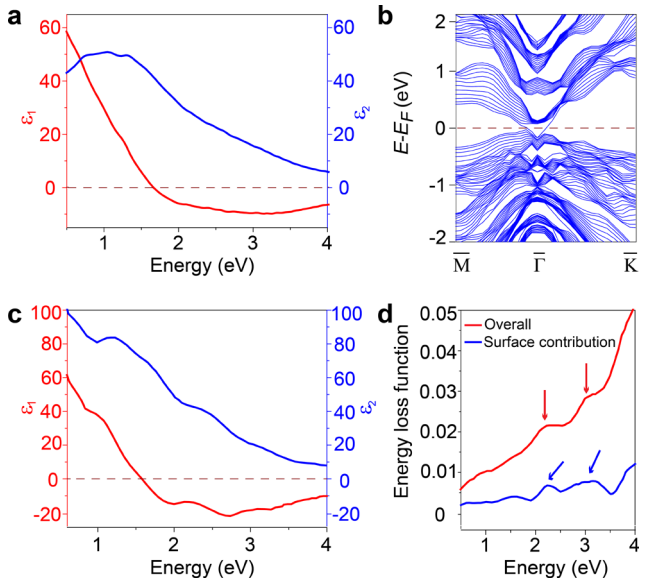

Figure 4. Dielectric function and energy loss function of Bi_2Te_3. (a) Experimental dielectric function data of Bi_2Te_3 obtained from ellipsometry measurements. (b) Calculated band structure of a 12 quintuple-layer (QL) Bi_2Te_3 slab (c) Calculated dielectric function and (d) energy-loss function of the same Bi_2Te_3 slab.

and a dielectric, the real part of the dielectric function (ε_1) must be negative.[39] The zero-cross frequency of ε_1 (where ε_1 changes from positive to negative) at 1.6 eV suggests that the surface plasmons of Bi_2Te_3 should resonate at energy values greater than 1.6 eV. The close agreement between the EEL spectra and the experimentally determined dielectric function supports the assignment of the observed peaks in EELS as surface plasmon resonances. We would like to mention that the relatively large imaginary part (ε_2) indicates that the plasmon modes may suffer from high losses.

It is well-known that such 3D TIs exhibit nontrivial metallic surface states due to the strong spin−orbit coupling (SOC) effect.[10] However, so far it is not clear how important the surface states and SOC are in terms of the plasmonic effects. To clarify the contribution of surface states to the negative dielectric function, we calculated the electronic band structure, dielectric function and energy-loss function (ELF) of a 12 quintuple-layer (QL) Bi_2Te_3 slab. Calculations of the electronic properties of the Bi_2Te_3 slab were made with the Vienna *ab initio* Simulation Package (VASP) (see Supporting Information for more details). The frequency-dependent, complex dielectric function of the Bi_2Te_3 slab was also calculated. As shown in Figure 4b, the topological surface states obtained are near the Fermi level, making the system gapless. The calculated electronic band structures agree well with those published earlier in literature[10] and thus validate our model, which was used to derive its dielectric function. The calculated dielectric function of the Bi_2Te_3 slab qualitatively agrees well with the experimental spectra, as shown in Figure 4c. The calculated zero-cross frequency of ε_1 is 1.6 eV as well, thus fulfilling the requirement to support surface plasmons.

The ELF describes the spectral density of the intrinsic plasmonic excitations.[40,41] The simulated overall ELF spectrum (Figure 4d) shows two energy-loss peaks at 2.1 and 3.0 eV that agree well with the experimentally observed center modes in EELS. The edge mode is not involved in this calculation due to the application of the periodic boundary condition. The effects of surface states were elucidated by separating out the contributions of surface states and bulk states in the ELF, and we still observed prominent peaks at the same energies due to the contribution of surface states. The contribution of surface states was further verified by calculations which show that the dielectric function and peak energies in ELF (see Figure S5) are almost thickness-independent when the thickness is larger than 9 QL. To further clarify the effects of the SOC on the dielectric function and ELF of Bi_2Te_3, we performed calculations for a Bi_2Te_3 slab without considering SOC, where we found a blue shift of the zero-cross frequency of ε_1 to 1.9 eV and vanishing of the peaks in ELF (see Figure S6). We thus conclude that strong SOC and surface states are responsible for the negative dielectric function of Bi_2Te_3, which provides the condition for the surface plasmon modes to exist in the visible range.

In conclusion, we identified and mapped multiple surface plasmon modes with energies that cover the entire visible range in Bi_2Te_3 nanoplates using TEM-based EELS and CL spectroscopy. A nontrivial "breathing mode" surface plasmon was also supported in the hexagonal nanoplates. Calculations showed that the interplay between spin−orbit coupling induced metallic surface states and the bulk states in the Bi_2Te_3 topological insulator gives rise to surface plasmons in the visible range. By resolving the spatial dependence of various plasmon modes in single Bi_2Te_3 nanoplates and clarifying the relationship with spin−orbit coupling, it provides the blueprint for the search for novel plasmonic nanocrystals.

■ ASSOCIATED CONTENT

Supporting Information

The Supporting Information is available free of charge on the ACS Publications website at DOI: 10.1021/acs.nanolett.5b03966.

Experimental and simulation details, additional sample characterizations, size-dependent EELS, calculated thickness-dependent dielectric function and ELF, additional SOC effect clarification, SEM and AFM images and a UV−Vis spectrum (PDF)

■ AUTHOR INFORMATION

Corresponding Author

*(K.P.L.) E-mail: chmlohkp@nus.edu.sg.

Notes

The authors declare no competing financial interest.

■ ACKNOWLEDGMENTS

K.P.L. and M.B. acknowledge the National Research Foundation funded CRP program "Plasmonic-Electronics: New Generation of Devices to Bypass Fundamental Limitations" (Award No. NRF-CRP 8-2011-07). C.-W.Q. acknowledges the financial support from A*STAR Pharos Programme (Grant No. 152 70 00014, with Project No. R-263-000-B91-305). H.L. acknowledges the Singapore National Research Foundation for the support under NRF Award No. NRF-NRFF2013-03. A.R. acknowledges NRF CRP (NRF-CRP 8-2011-06) and MOE-AcRF Tier-2 (MOE2015-T2-1-099). M.Z. sincerely thanks Prof. Antonio H. Castro Neto, Prof. Joel K. W. Yang, Prof. Jiong Lu, Prof. Qiaoliang Bao, Prof. Yi Zheng, and Dr. Tao Wang for fruitful discussions.

DOI: 10.1021/acs.nanolett.5b03966
Nano Lett. 2015, 15, 8331−8335

REFERENCES

(1) Barnes, W. L.; Dereux, A.; Ebbesen, T. W. *Nature* **2003**, *424* (6950), 824−830.
(2) Atwater, H. A.; Polman, A. *Nat. Mater.* **2010**, *9* (3), 205−213.
(3) Liao, H.; Nehl, C. L.; Hafner, J. H. *Nanomedicine* **2006**, *1* (2), 201−208.
(4) Punj, D.; Mivelle, M.; Moparthi, S. B.; van Zanten, T. S.; Rigneault, H.; van Hulst, N. F.; Garcia-Parajo, M. F.; Wenger, J. *Nat. Nanotechnol.* **2013**, *8* (7), 512−516.
(5) De Angelis, F.; Patrini, M.; Das, G.; Maksymov, I.; Galli, M.; Businaro, L.; Andreani, L. C.; Di Fabrizio, E. *Nano Lett.* **2008**, *8* (8), 2321−2327.
(6) Liu, L.; Han, Z. H.; He, S. L. *Opt. Express* **2005**, *13* (17), 6645−6650.
(7) Nikitin, A. Y.; Guinea, F.; Garcia-Vidal, F. J.; Martin-Moreno, L. *Phys. Rev. B: Condens. Matter Mater. Phys.* **2011**, *84* (16), 161407.
(8) Saleemi, M.; Toprak, M. S.; Li, S.; Johnsson, M.; Muhammed, M. *J. Mater. Chem.* **2012**, *22* (2), 725−730.
(9) Shen, J.-J.; Zhu, T.-J.; Zhao, X.-B.; Zhang, S.-N.; Yang, S.-H.; Yin, Z.-Z. *Energy Environ. Sci.* **2010**, *3* (10), 1519−1523.
(10) Zhang, H.; Liu, C.-X.; Qi, X.-L.; Dai, X.; Fang, Z.; Zhang, S.-C. *Nat. Phys.* **2009**, *5* (6), 438−442.
(11) Chen, Y. L.; Analytis, J. G.; Chu, J.-H.; Liu, Z. K.; Mo, S.-K.; Qi, X. L.; Zhang, H. J.; Lu, D. H.; Dai, X.; Fang, Z.; Zhang, S. C.; Fisher, I. R.; Hussain, Z.; Shen, Z.-X. *Science* **2009**, *325* (5937), 178−181.
(12) Di Pietro, P.; Ortolani, M.; Limaj, O.; Di Gaspare, A.; Giliberti, V.; Giorgianni, F.; Brahlek, M.; Bansal, N.; Koirala, N.; Oh, S.; Calvani, P.; Lupi, S. *Nat. Nanotechnol.* **2013**, *8* (8), 556−560.
(13) Ou, J.-Y.; So, J.-K.; Adamo, G.; Sulaev, A.; Wang, L.; Zheludev, N. I. *Nat. Commun.* **2014**, *5*, 5139.
(14) Hartschuh, A. *Angew. Chem., Int. Ed.* **2008**, *47* (43), 8178−8191.
(15) Sönnichsen, C.; Franzl, T.; Wilk, T.; von Plessen, G.; Feldmann, J.; Wilson, O.; Mulvaney, P. *Phys. Rev. Lett.* **2002**, *88* (7), 077402.
(16) Chen, J.; Badioli, M.; Alonso-Gonzalez, P.; Thongrattanasiri, S.; Huth, F.; Osmond, J.; Spasenovic, M.; Centeno, A.; Pesquera, A.; Godignon, P.; Zurutuza Elorza, A.; Camara, N.; de Abajo, F. J. G.; Hillenbrand, R.; Koppens, F. H. L. *Nature* **2012**, *487* (7405), 77−81.
(17) Fei, Z.; Rodin, A. S.; Andreev, G. O.; Bao, W.; McLeod, A. S.; Wagner, M.; Zhang, L. M.; Zhao, Z.; Thiemens, M.; Dominguez, G.; Fogler, M. M.; Neto, A. H. C.; Lau, C. N.; Keilmann, F.; Basov, D. N. *Nature* **2012**, *487* (7405), 82−85.
(18) García de Abajo, F. J. *Rev. Mod. Phys.* **2010**, *82* (1), 209−275.
(19) Kociak, M.; Stéphan, O. *Chem. Soc. Rev.* **2014**, *43* (11), 3865−3883.
(20) Nicoletti, O.; Wubs, M.; Mortensen, N. A.; Sigle, W.; van Aken, P. A.; Midgley, P. A. *Opt. Express* **2011**, *19* (16), 15371.
(21) Duan, H.; Fernández-Domínguez, A. I.; Bosman, M.; Maier, S. A.; Yang, J. K. W. *Nano Lett.* **2012**, *12* (3), 1683−1689.
(22) Chu, M.-W.; Myroshnychenko, V.; Chen, C. H.; Deng, J.-P.; Mou, C.-Y.; García de Abajo, F. J. *Nano Lett.* **2009**, *9* (1), 399−404.
(23) Schmidt, F.-P.; Ditlbacher, H.; Hohenester, U.; Hohenau, A.; Hofer, F.; Krenn, J. R. *Nano Lett.* **2012**, *12* (11), 5780−5783.
(24) Losquin, A.; Zagonel, L. F.; Myroshnychenko, V.; Rodríguez-González, B.; Tencé, M.; Scarabelli, L.; Förstner, J.; Liz-Marzán, L. M.; García de Abajo, F. J.; Stéphan, O.; Kociak, M. *Nano Lett.* **2015**, *15* (2), 1229−1237.
(25) Zhang, G.; Wang, W.; Lu, X.; Li, X. *Cryst. Growth Des.* **2009**, *9* (1), 145−150.
(26) Cha, J. J.; Koski, K. J.; Huang, K. C. Y.; Wang, K. X.; Luo, W.; Kong, D.; Yu, Z.; Fan, S.; Brongersma, M. L.; Cui, Y. *Nano Lett.* **2013**, *13* (12), 5913−5918.
(27) Liou, S. C.; Chu, M. W.; Sankar, R.; Huang, F. T.; Shu, G. J.; Chou, F. C.; Chen, C. H. *Phys. Rev. B: Condens. Matter Mater. Phys.* **2013**, *87* (8), 085126.
(28) Nelayah, J.; Kociak, M.; Stéphan, O.; García de Abajo, F. J.; Tencé, M.; Henrard, L.; Taverna, D.; Pastoriza-Santos, I.; Liz-Marzán, L. M.; Colliex, C. *Nat. Phys.* **2007**, *3* (5), 348−353.
(29) Bosman, M.; Keast, V. J.; Watanabe, M.; Maaroof, A. I.; Cortie, M. B. *Nanotechnology* **2007**, *18* (16), 165505.
(30) Raether, H. *Excitation of Plasmons and Interband Transitions by Electrons*; Springer: Berlin and Heidelberg, Germany, 1980.
(31) Hohenester, U. *Comput. Phys. Commun.* **2014**, *185* (3), 1177−1187.
(32) Krug, M. K.; Reisecker, M.; Hohenau, A.; Ditlbacher, H.; Truegler, A.; Hohenester, U.; Krenn, J. R. *Appl. Phys. Lett.* **2014**, *105* (17), 171103.
(33) Gómez, D. E.; Teo, Z. Q.; Altissimo, M.; Davis, T. J.; Earl, S.; Roberts, A. *Nano Lett.* **2013**, *13* (8), 3722−3728.
(34) Giannini, V.; Fernández-Domínguez, A. I.; Sonnefraud, Y.; Roschuk, T.; Fernández-García, R.; Maier, S. A. *Small* **2010**, *6* (22), 2498−2507.
(35) Bosman, M.; Ye, E.; Tan, S. F.; Nijhuis, C. A.; Yang, J. K. W.; Marty, R.; Mlayah, A.; Arbouet, A.; Girard, C.; Han, M.-Y. *Sci. Rep.* **2013**, *3*, 1312.
(36) Schmidt, F.-P.; Ditlbacher, H.; Hohenester, U.; Hohenau, A.; Hofer, F.; Krenn, J. R. *Nat. Commun.* **2014**, *5*, 3604.
(37) Link, S.; El-Sayed, M. A. *J. Phys. Chem. B* **1999**, *103* (21), 4212−4217.
(38) Lee, K.-S.; El-Sayed, M. A. *J. Phys. Chem. B* **2006**, *110* (39), 19220−19225.
(39) Maier, S. A. *Plasmonics: Fundamentals and Applications*; Springer: New York, 2007.
(40) Onida, G.; Reining, L.; Rubio, A. *Rev. Mod. Phys.* **2002**, *74* (2), 601−659.
(41) Stauber, T. *J. Phys.: Condens. Matter* **2014**, *26* (12), 123201.

DOI: 10.1021/acs.nanolett.5b03966
Nano Lett. 2015, 15, 8331−8335